Damage of Semicrystalline Polyamide 6 Assessed by 3D X-Ray Tomography: From Microstructural Evolution to Constitutive Modeling

L. LAIARINANDRASANA, T. F. MORGENEYER, H. PROUDHON, C. REGRAIN

MINES Paristech, Centre des Matériaux–CNRS UMR 7633, BP 87, 91003 Evry Cedex, France

Received 3 October 2009; revised 3 March 2010; accepted 9 April 2010
DOI: 10.1002/polb.22043
Published online in Wiley InterScience (www.interscience.wiley.com).

ABSTRACT: In this study an attempt is made to link the damage and microstructural evolution of semicrystalline polymers, in particular polyamide 6, to the macroscopic material behavior during tensile and creep tests. Tensile specimens, removed before failure were seen to have undergone striction. They were examined using synchrotron radiation tomography. These samples showed elongated axisymmetric columns of voids separated by thin ligaments of material. These observations were confirmed and refined through a cryofractography experiment of a different tensile sample, stopped before failure. An attempt was made to obtain quantitative data about void volume fraction and morphology through image analysis. © 2010 Wiley Periodicals, Inc. J Polym Sci Part B: Polym Phys 48: 1516–1525, 2010

KEYWORDS: creep; damage zone; fracture; mechanical properties; modeling; necking; polyamides; porosity; semicrystalline polymers; tensile tests; voids; X-ray tomography

INTRODUCTION Structural polymers are more and more used in engineering components submitted to thermomechanical loadings and their mechanical behavior is a key factor in the design of such components.

The mechanical properties depend on the kind of polymeric material but also on the range of strain rates imposed by the loading conditions in service. This article deals with Polyamide 6 (PA6) but the essential results and conclusions of the investigation are expected to extend to semicrystalline polymers in general. The sample of polymeric material, that was initially free of macroscopic geometrical defects, was submitted to quasistatic (monotonic tensile) or static (creep test) loading.

When tested under both kinds of loading, PA6 samples eventually show necking. The extension of the neck is accompanied by whitening of the concerned material. Research works[1–5] on whitening generally agree that this phenomenon is due to the presence of voids in the highly deformed polymeric material. Whitening appears in the vicinity of a geometrical defect, for instance a change in the cross-sectional area along the sample. In the literature, numerous studies on cold drawing of polymers are discussed concerning flat samples that either experienced necking during deformation[6,7] or exhibited pre-existing geometrical defects (cut outs, machined notches).[7] The neck propagation is reported to induce self-excited oscillation of the deformation process named as "thermal runaway" that depends on the loading rate under monotonic tensile tests.[7–10] Pakula and Fischer[7] analyzed the cold drawing at constant stress, similar to creep tests reported here. In these cases, the apparition of cavities is generally attributed to temperature variation between the bulk and the drawn polymers. Butler,[6] with the help of small- and wide-angle X-ray scattering (SAXS and WAXS, respectively) patterns studied the evolution of voiding during cold drawing on Polyethylene. It was seen that a locking phenomenon (triaxiality) of the interlamellae phase played a major role in the void nucleation, which appears at the yield point of the stress-strain curve.

Other studies on semicrystalline polymers[2,11–13] were carried out on notched round bars (controlled geometrical defect) with various notch root radii to represent the shape of the necked specimens. Interrupted tests during monotonic tensile loading on these notched round bars were performed by Challier[2,11] on PVDF and Boisot[12] on PA11, respectively. Longitudinal cuts observed by SEM allowed the evolution of the void volume fraction and the location of it is the maximum value to be estimated. Similar investigations were carried out by Regrain[13] on PA6 under creep loading. The main conclusions of these last works were as follows:

- The presence of initial void volume fraction in all tested materials: about 1% apart from "model" PVDF where the estimates were as high as 10%.
- The presence of a substantial void volume fraction in the whitened zone after interrupted tests (observed by SEM).
- The size and the shape of voids depended on the initial notch root radius.
- The stress state in the minimum cross section during necking is highly multiaxial leading to significant spherical void growth.

Correspondence to: L. Laiarinandrasana (E-mail: lucien.laiarinandrasana@mines-paristech.fr)
Journal of Polymer Science: Part B: Polymer Physics, Vol. 48, 1516–1525 (2010) © 2010 Wiley Periodicals, Inc.

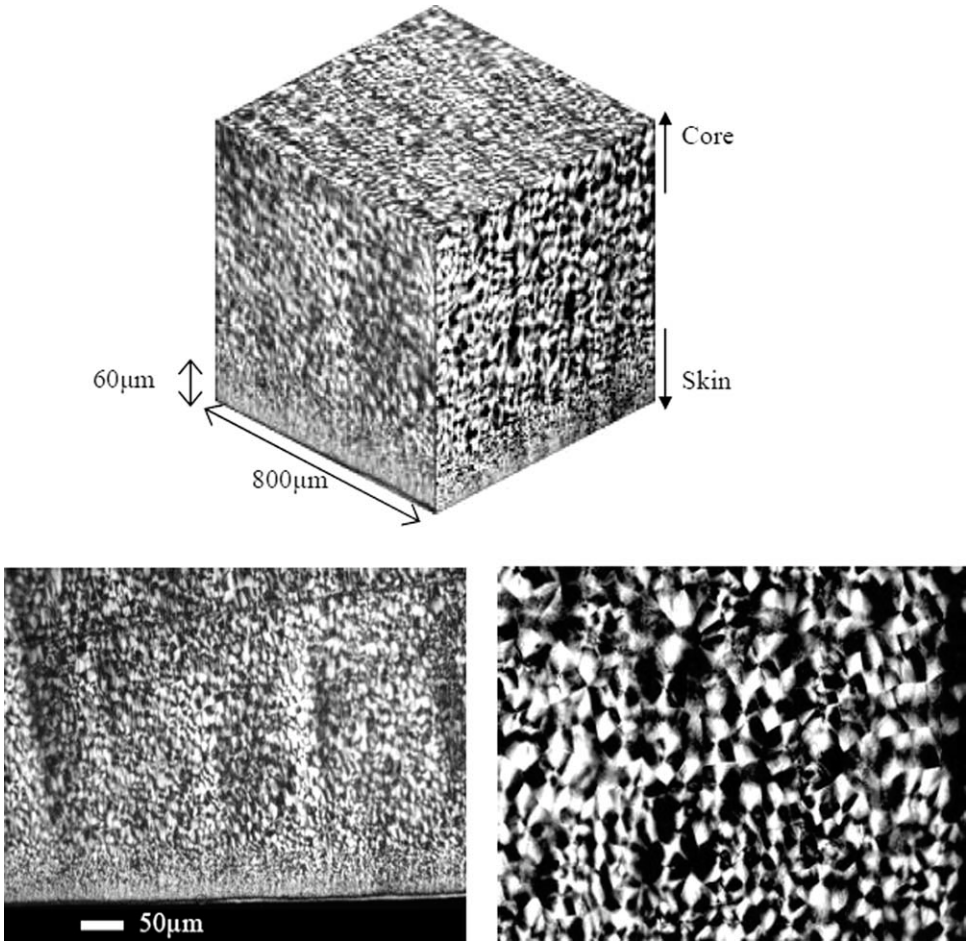

FIGURE 1 Optical microscope examinations of the size distribution of spherulites–Skin effect. (Adapted after [6])

- The higher the value of notch root radius, the lower the stress triaxiality ratio and the more concentrated in the center of the minimum cross section was the maximum void volume fraction.

Modeling of the mechanical behavior of such materials should take into account the void volume fraction and evolution, so as to determine any variation in volume.[14] To this end, the knowledge of the statistical data on these voids is essential. Parameters such as the mean values and the associated standard deviations corresponding to the number, size, and shape of these voids are needed.

Historically, two-dimensional (2D) surface imaging techniques, such as optical and electron microscopy have been used to reveal damage and fracture micromechanisms.[3,11,12] With recent developments in synchrotron radiation computed tomography (SRCT) it has become possible to visualize fracture mechanisms within materials at the submicron scale in three dimensions (3D).[15] Valuable input and validation data for void growth models applied to metallic material has been obtained through SRCT.[16,17] To the best of the authors' knowledge it is the first time SRCT has been applied to PA6 semicrystalline polymers to observe damage in 3D.

The aim of this article is therefore to examine the microstructure of the PA6 at particular periods during the testing, and to draw some basic conclusions for mechanical modeling. First, microscopic examinations of the as received PA6 material are discussed in Section 2. Then the experimental procedure of interrupted tests producing necked specimens, and the examinations of the necked volume with the help of SRCT are presented in Section 3. Section 4 deals with the results in terms of images, followed by the statistical treatment of data issued from the tomography technique. The essential figures are compared with the ones obtained in Section 2. The sequence of micromechanisms of the deformation of the PA6 polymer together with the void nucleation and growth are then discussed, so as to highlight possible consequences from the mechanical modeling point of view.

AS RECEIVED PA6 MATERIAL: MICROSTRUCTURE

The PA6 material under study was provided by Angst and Pfister as 610 mm × 1230 mm flow molded plates with 10 mm in thickness.[13,18] Physicochemical properties were determined on some samples of this PA6 material. The glass transition temperature $T_g = 53$ °C, the melting point $T_F = 219$ °C and crystallinity index $z = 43\%$ were obtained with the

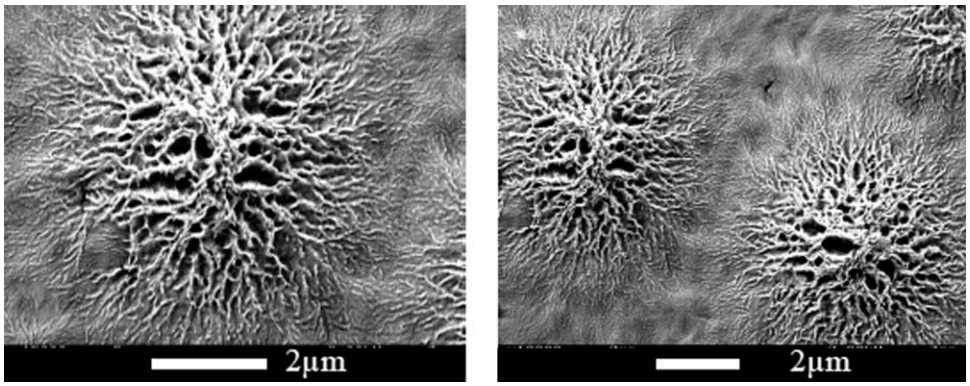

FIGURE 2 SEM observation of the spherulitic microstructure on etched surfaces. (Adapted after [6,11])

help of Modulated Differential Scanning Calorimeter (MDSC). The Young's modulus $E = 2850$ MPa was estimated with the initial slope of the stress-strain curve.

PA6 is a semicrystalline polymer. To reveal the expected spherulitic microstructure, a sample was cut with a cryomicrotome. Optical microscope observations in the three main directions are shown in Figure 1. Regular equiaxed spherulites can be seen with a clear skin effect: the first 60 μm from the surface exhibit small spherulites, compared with those located in the center. Because of this effect, all of the following examinations were done in the central part of the sample.

Samples were also examined by Scanning Electron Microscopy (SEM) after chemical etching. This latter partly eliminated the amorphous phase. Only the "skeleton" of the crystallite parts remained, giving an idea of the spherulite size. The results are illustrated in Figure 2 focusing on one and two spherulite(s) to show their typical morphology. About 50 spherulites have been examined; their mean diameter is 6 μm.

To investigate whether an initial void volume fraction is present in the as received material, the cryofractography technique was used.[2,3,18] It consists in plunging the sample in liquid nitrogen at -196 °C and subsequently breaking it in a brittle manner. Here, the glass transition temperature of the material is high enough so that the microstructure is supposed to be frozen at -196 °C. Examinations of the fracture surface then reveal the initial microstructure, that is, without deformation. Figure 3 shows two pictures of the surface at different magnifications. Figure 3(a) reveals that the brittle fracture was interspherulitic. Indeed the fracture surfaces show some circular patterns the size of which is similar to the spherulitic mean diameter. At submicrometer scale [Fig. 3(b)] the fracture surface exhibited porosity. The presence of such a porosity raises the question of whether it was formed during the cryofracture operation. For instance, Parrish and Brown[19] found that nitrogen and liquid air at nitrogen temperature, that is, temperature of the sample during the cryofracture operation were crazing agents for polycarbonate, polyethylene terephtalate, and PMMA. However, this phenomenon was observed on thin films of amorphous polymers, the swelling of which could cause crazing of the whole cores. Kambour,[4] in a review of crazing in thermoplastics, reported that crazing does not occur immediately. Long delays in craze formation were observed when changes of stress level took place during the test. It seems then that the diffusion rate of the nitrogen is so low that it cannot interfere with the microstructure examined in the center of a thick sample as observed here. Consequently, the observed porosity in this article is assumed to be pre-existing.

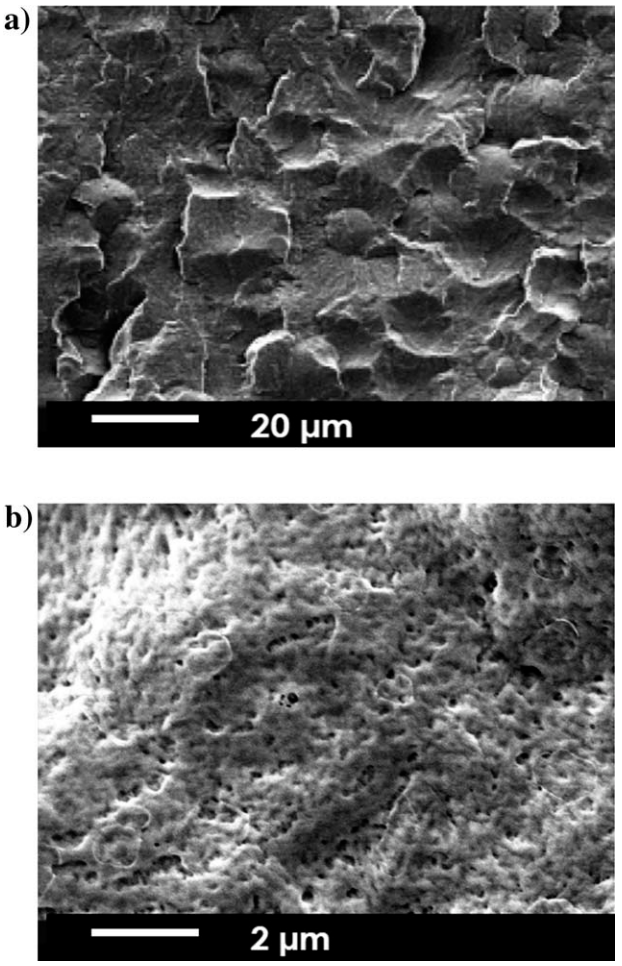

FIGURE 3 Cryofractured surfaces SEM observations, (a) interspherulitic fracture surface (b) presence of initial porosity.

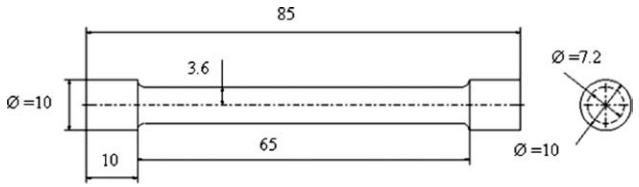

FIGURE 4 Scheme of the round bar specimen (ASTM D638-91 and D2990, all dimensions in mm).

This assumption however does not affect the general comments on SRCT observations.

By performing image analysis on many cryofractured surface pictures, quantification of the voided surface (black) normalized to the total surface of the examined area, was carried out. Then, by assuming isotropic distribution in size and dispersion, the void surface fraction was considered as the void volume fraction (noted as f_0). The initial void volume fraction was then estimated at 1 to 2% and the void mean diameter is about 0.1 μm.

EXPERIMENTAL PROCEDURE

Interrupted Tests

The PA6 under study shows necking during both tensile and creep tests.[13,18] Additionally, the necked zone appears whitened. Whitening is generally related to voids for which volume fraction is rather high (ten's of percent).[1] To investigate the microstructure of the material within the necking zone, interrupted tests were carried out. To this end, round bar specimens were machined (Fig. 4), following ASTM D638-91 and D2990. They were extracted from the center of the plate to avoid the aforementioned skin effect.

During monotonic tensile loading, necking appears at the maximum load of the stress-strain curve, whereas for creep tests, it begins at the onset of the "tertiary creep" (increase of the creep strain rate). Figure 5 shows when tests were interrupted to obtain a similar whitened necking region of the specimen, in both stress-strain and creep strain experiments. As creep tests are time consuming, the observations in this article were carried out essentially on necked zones obtained in tensile tests.

X-Ray Tomography Imaging

To investigate the shape of the voids within the necked region of the PA6 sample, X-ray tomography experiments were carried out at the beam line ID19 of the European Synchrotron Radiation Facility located in Grenoble (France). The tomographic setup was rather classical with a monochromatic parallel beam tuned at 20 keV going through the sample before hitting the scintillator. Attenuated X rays were then transformed into visible light which was collected by a 2048 $\times$ 2048 pixels Frelon

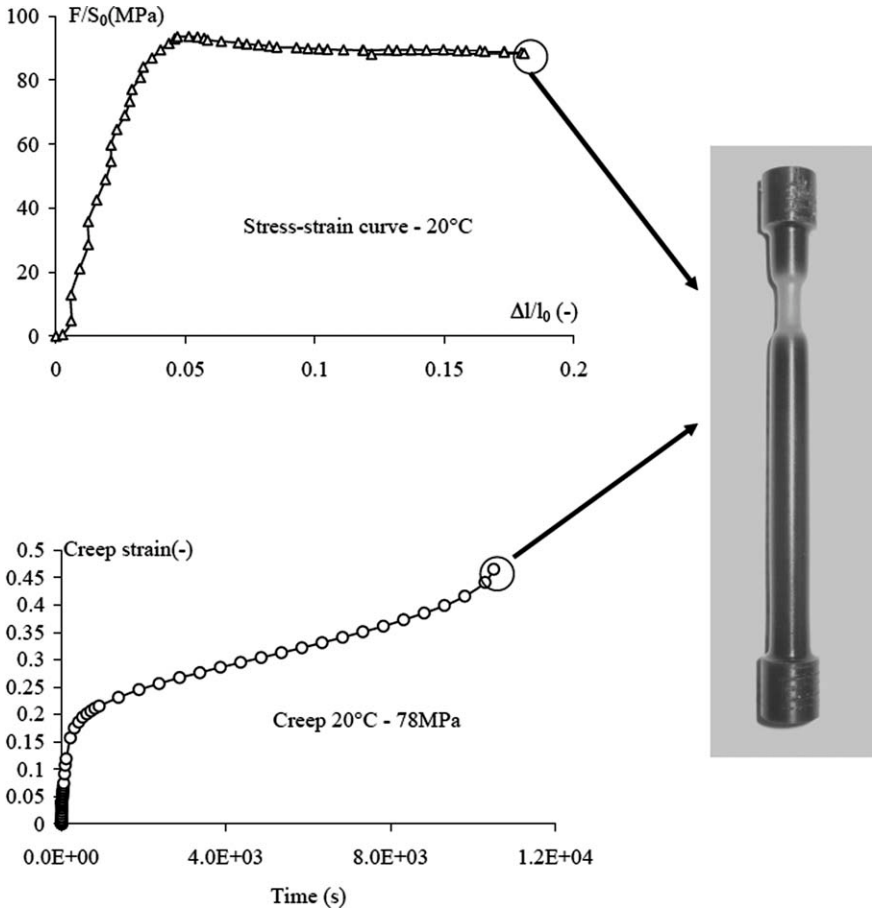

FIGURE 5 Interrupted tests to obtain necked and whitened zone.

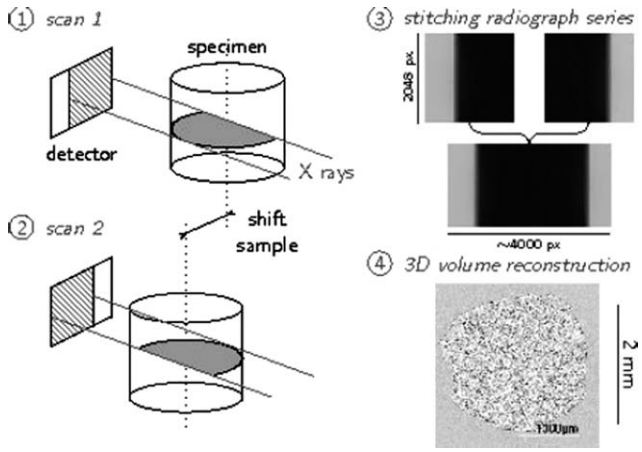

FIGURE 6 Illustration of the stitching technique used to image bigger samples.

CCD camera to form a radiograph. A tomographic scan corresponded to a large set of radiographs of the sample (typically 1500), recorded over a 180° rotation. The distance from the sample to the camera was set to 100 mm which was expected to give a reasonable amount of phase contrast to highlight voids present inside the sample.

The size of the isotropic voxels in the reconstructed volumes was 0.7 μm. With a parallel beam, the specimen size is usually restricted to the product of the number of pixels (2048 here) by the pixel size (0.7 μm) which, would give here 1.4 mm. To image a bigger sample without compromising the resolution (provided the X-ray attenuation is low enough to give a good signal over noise ratio), radiograph stitching can be used, also called 'half-acquisition' (see Fig. 6) available at ID19.[20] The principle of this technique relies on two successive tomographic scans having the rotation axis shifted with respect to the center of the sample. Each scan is carried out with a higher number of projections (usually twice as many as for a normal scan) to preserve the resolution on the outer edges of the sample. Between the two scans, the sample is shifted horizontally. Before proceeding to the reconstruction, the two series of radiographs are stitched together to represent a single data set (each radiograph will then roughly be 2000 × 4000 pixels). 3D reconstruction is then conducted as usual with a filtered back projection algorithm. If the stitching process is done properly (image correlation on the overlapping zone must be carried out), the reconstruction does not present any particular artifacts. Volumes reconstructed this way are much bigger in size as they represent four times more material with the same resolution.

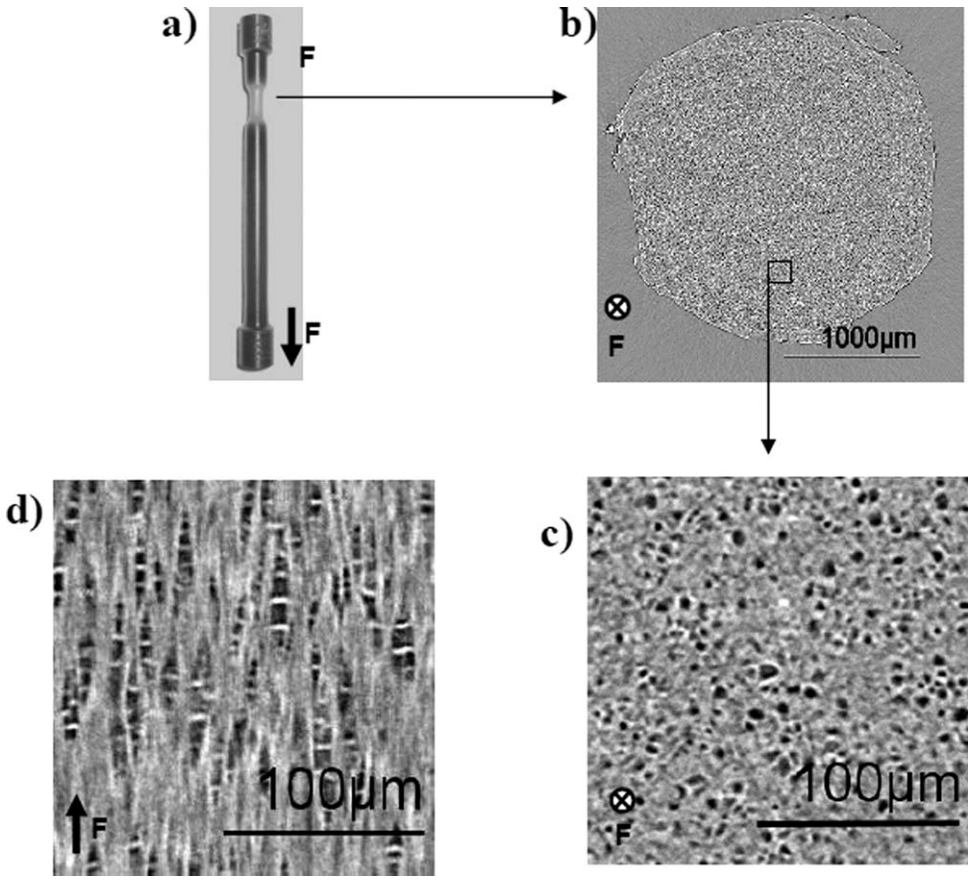

FIGURE 7 (a) PA6 tensile sample with whitened necking area (b) 2D section of the tomography data of the necking area normal to loading (c) zoom of an area of b at higher magnification (d) 2D tomography section normal to section c showing elongated voids (Arrows F indicate the former tensile testing direction).

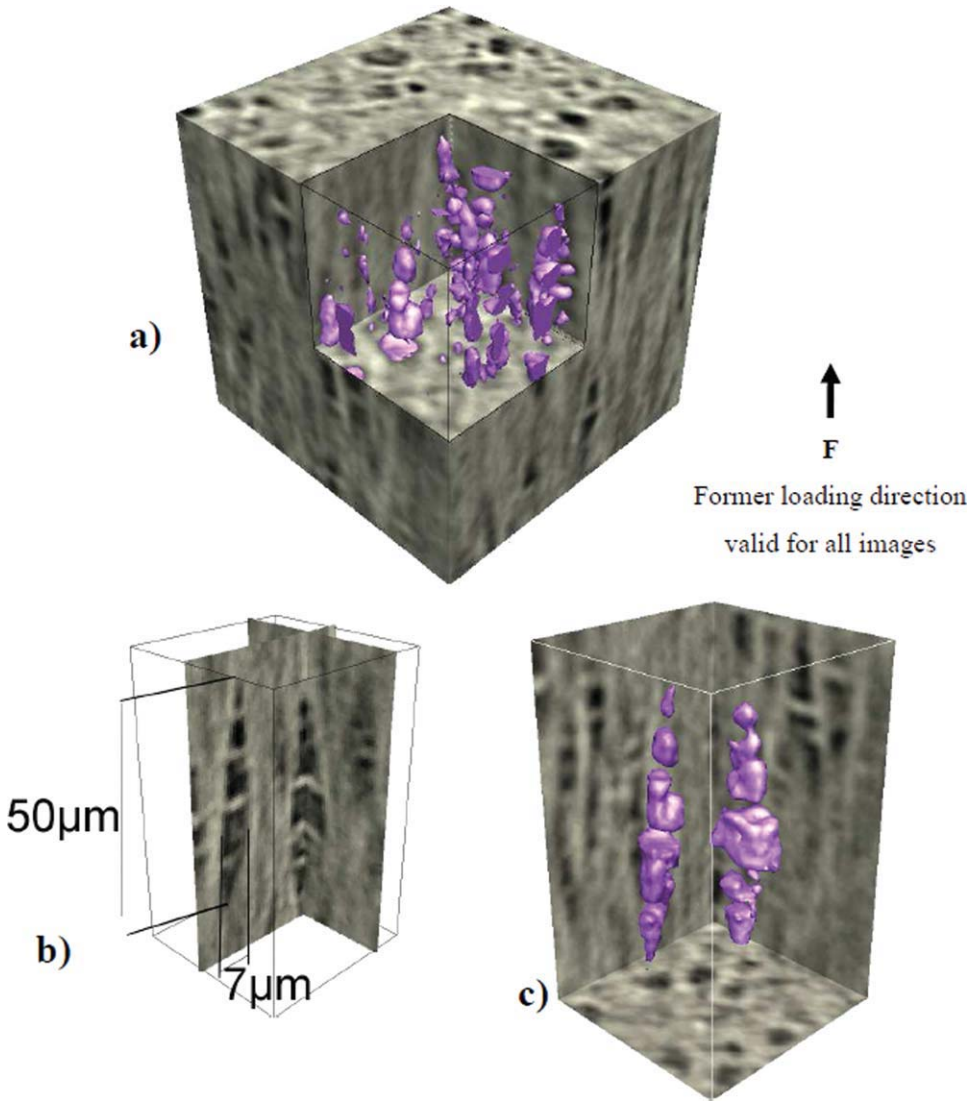

FIGURE 8 Images within the necked zone of the samples (a) 3D rendering of a 100 × 100 × 100 microns region. The voids have been contoured by an isosurface, (b) orthogonal sections of two typical void columns, (c) 3D rendering of the two void columns characterized by elongated shape of the voids with small nonbroken segment of matter (walls).

Image Analysis Procedures

An in-house matlab code and ImageJ software were used.[21] The void volume fraction in the arrested test has been determined in a volume of 490 μm × 490 μm × 184 μm. First a 3D filter was applied to address noise issues, and segmentation of the voids via gray value thresholding was then carried out. Void columns were morphologically agglomerated using a directional dilation in former loading direction coupled with void reconstruction.

MICROSTRUCTURES AND DAMAGE IN THE NECKING ZONE

3D Imaging of the Necking Zone

The necked zone of the PA6 specimen was reduced in diameter to roughly 2 mm through cutting and scanned by X-ray tomography (see Fig. 7) using image stitching leading to a 3D data set of 32 GB (4000 × 4000 × 2000 pixels). Each pixel has a gray value between 0 (black) and 255 (white) closely related to the local density of the material. The reconstructed value of the pixel is indeed the linear X-ray attenuation coefficient, which depends mostly on the average atomic number on a pixel (constant for single phase material) and on the local density.

Voids are clearly visible on slices extracted from the 3D data set and appear in black color due to phase contrast. Figure 7(a) shows the tensile sample of an interrupted test with the whitened necking region. In Figure 7(b), a 2D image of the cross section of the necking region normal to the former loading direction obtained by tomography can be seen. Figure 7(c) shows an area of the same section but at higher magnification.

It can be observed that the voids (in black) have round mostly axisymmetric cross sections of different diameters in

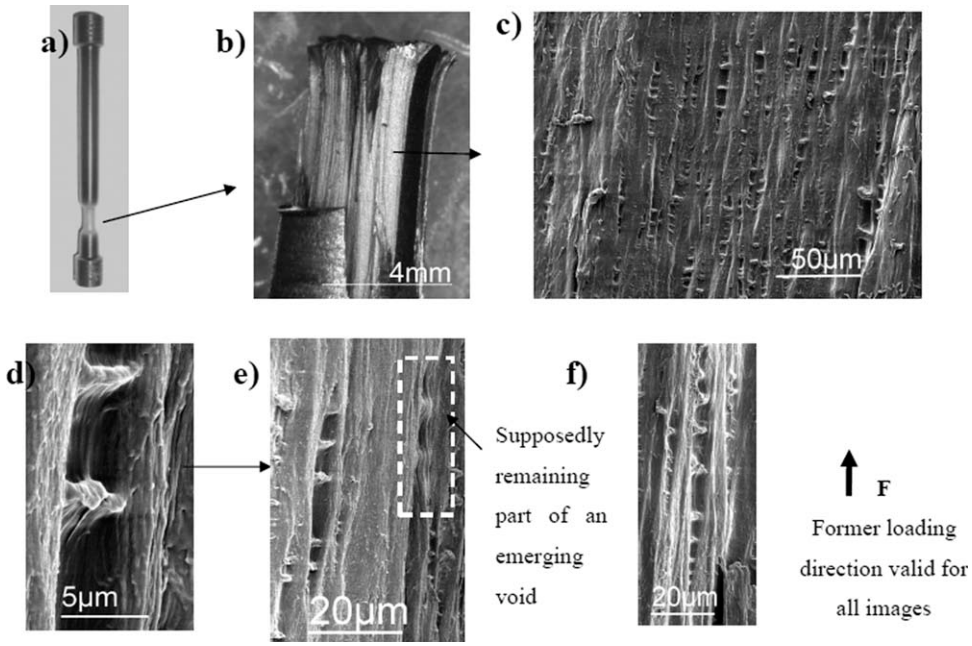

FIGURE 9 Examinations of cryo-fractured surfaces (a) PA6 tensile sample with whitened necking area (b) macroscopic optical microscope image of the cryofractured surface (c) SEM image of same section at higher magnification (d) SEM image of a part of a void cluster showing a rest of a wall (e) SEM image of the same void cluster as in d at lower magnification; emerging void column (f) SEM image of a void cluster and voids with round and sharp corners.

this plane. The maximum diameter is about 10 μm. Figure 7(d) shows a 2D section of the material obtained by tomography in a plane normal to the specimen radius. Voids clearly exhibit a very distinct elongated shape in the loading direction. They are arranged in columns and are separated by a thin layer of unbroken ligament material that the authors name "walls" hereafter. This is an interesting feature, which, to the best of the authors' knowledge, has not been reported before and highlights the potential of using X-ray tomography to study damage in those materials.[22]

Selected voids were contoured in 3D in Figure 8(a) whereas in Figure 8(b) a reconstruction of two typical void columns through orthogonal sections is depicted. A 3D rendering of these two void columns is illustrated in Figure 8(c). The elongated shape is clearly shown, consisting of several voids separated by walls. It is to be noted that the outer voids have a cone shape while the intermediate voids are more cylinder like shaped. The sharp outer ends of the voids seem then to be indicative for void growth following one direction. Alternatively, intermediate voids show triaxial growth.

Cryofractography of the Necking Region

To avoid misunderstandings due to possible artifacts of the tomography technique (image reconstruction, degradation of the material due to heating from X-ray beam), a cryofractography experiment was carried out on an interrupted tensile test [see Fig. 9(a)]. To this end, a small notch was cut in the necking region. The sample was cooled in liquid nitrogen for 15 min, and subsequently fractured by loading in bending. The sample was coated with a metallic layer for SEM observation. The sample broke in a brittle manner in the tensile loading direction with a 'fiber like' structure of the fracture surface [see Fig. 9(b)].

Figure 9(c) shows a SEM image of the fracture surface that is oriented normal to the sample radius. Similar void columns as observed by tomography can be discerned. The tomography observation is therefore validated. Reciprocally, it should be mentioned, that SCRT technique resolution does not allow observing voids with a diameter of 100 nm. The comparison between Figures 7(d) and 9(c) confirms that both cryofractography and SRCT techniques lead to the same microstructural morphology. This reinforces the observation shown in Figure 3(b) examinations on cryofractured surfaces and the resulting initial void volume fraction value.

The walls between the voids of the void column are clearly discernable. Figure 9(d) shows a part of void column at higher magnification. The typical wall thickness seems to be $\sim$2 μm. Figure 9(e) shows the same void at lower magnification.

The voids in the middle of the column are clearly larger than at the outer ends. As revealed by the tomography observations, the outer voids have a cone shape with a sharply angled end while the middle voids have more of a cylinder shape.

At the right end of Figure 9(e), a feature can be observed that is supposed to be an emerging void column. The walls in this case are still rather thick $\sim$5 μm and the void dimples are elongated but are smooth and have no sharp edges

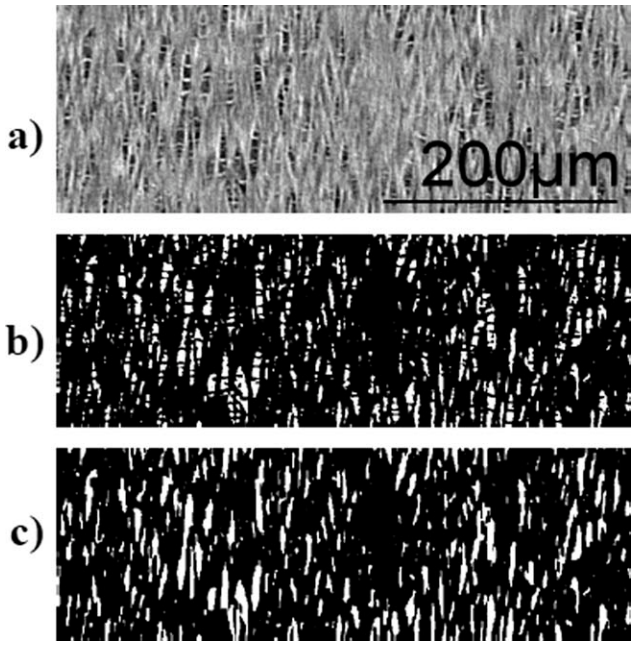

FIGURE 10 (a) "untreated" 2D section of the tomography data, (b) binarized volume showing voids in white and the material in black, (c) binarized material where gaps caused by walls are closed through directional dilatation

yet. Figure 9(f) shows another void column the individual voids of which are either round or sharply edged.

Image Processing Results: Statistical Data

In this section the results of a first attempt for a physically meaningful morphological analysis of tomography data is presented. A limiting factor of the validity of the analysis is the resolution used in the tomography observation. From the SEM cryofractography observations it becomes clear that all features cannot be resolved through tomography. Additionally, noise issues may be expected. Especially very small voids (<1 μm) cannot be clearly imaged. The results of the analysis are greatly influenced by filtering and thresholding where parameters can only be set somewhat arbitrarily by eye. Bearing these limitations in mind, the results will be interpreted with respect to possible void growth mechanisms.

Figure 10(a) shows a 2D section of the analyzed volume. A 2D section of the binarized volume is shown in Figure 10(b). It can be seen that the walls between the voids in one column are also discernable in the binarized image. The void volume of the binarized data set is $\sim$14% (see Table 1). The average Feret[23] dimensions of the voids on the 2D section presented here are also given in Table 1. It can be seen that the individual voids are more elongated in loading direction than in the radial direction with an aspect ratio of $\sim$2.

The average dimensions of the void columns were measured in 3D. A morphological directional dilation of the voids in loading direction was carried out. Figure 9(c) shows the results of the directional dilation that has produced an agglomeration of the voids in columns. The gaps caused by the walls were closed after the dilation and it is now possible to get some quantification of the mean parameters of the void columns. Their mean Feret dimensions and aspect ratios have been quantified on the shown 2D section in two dimensions. It turns out that the voids are then substantially more elongated in the loading direction than in the radial direction with an average aspect ratio of 3.2.

DISCUSSION

Elongated voids aligned in void columns have clearly been observed using SRCT and via cryofractography in the whitened necking area of an arrested PA 6 tensile sample for the first time. The voids in columns are separated through $\sim$2 μm thick unbroken ligaments that are named walls. The amount of void volume fraction was measured to be 14% in the necking area and voids were elongated in the loading direction, with an average void aspect ratio of 2 considering individual voids and of 3.2 for agglomerated void columns (Table 1). These voids may have different origins. Although the present observations did not focus on the void formation, the main controlling parameters reported in the literature can be recalled here: (i) temperature variation due to self heating during the deformation process, that may induce thermal runaway[7–10]; (ii) an increase in stress triaxiality in the section of the shoulder of the neck causing a locking phenomenon in the interlamellar phase[6]; (iii) pre-existing porosity that grows due to the triaxial stress state[11]; (iv) decohesion at the particle/matrix interface, for example, at fillers like carbon black. In this study the initial void diameter is estimated at about 0.1 μm, which cannot be observed by SRCT at the present time due to resolution limitations. SAXS and IR camera techniques would be more efficient for relevant observations whereas *in situ* SRCT test would be able to catch the evolution of the void shape: from spherical void growth to elongated voids.

In the literature, oscillation phenomena were observed in polymers during neck extension (cold drawing). In this study, although a rise of temperature was observed in the neck during some tensile tests,[24] the thermal runaway did not take place. The acceleration of the neck extension as mentioned by Pakula and Fischer[7] for cold drawing at constant stress was indeed observed in this study. This was interpreted as tertiary creep in[24] and the "duration" of this tertiary stage of creep depended on the initial notch root radius of the specimen.

The present observations did not give any information about the craze formation and the void coalescence leading to a macrocrack. The formation of the void columns and walls is still not clear. Furthermore the coalescence mechanisms of the void columns are still unknown. It would also be interesting to know how and at what point the craze will form. This highlights that there is still a mayor potential for observations via SRCT to better understand the damage mechanisms in semicrystalline polymers. *In situ* experiments would certainly be the richest form to follow the evolution of damage in terms of shape, distribution, and void volume fraction.

TABLE 1 Image Analysis Void Measurements

Voids			Void Agglomeration into Columns by Morphological Image Processing		
$f_v \sim 14\%$			$f_v \sim 17\%$		
Mean Feret Dimensions of Voids		Average Aspect Ratio	Mean Feret Dimensions of Agglomerated Voids		Average Aspect Ratio
Loading direction	Radial direction	Loading direction/ radial directions	Loading direction	Radial direction	Loading direction/ radial directions
6.3 μm	2.8 μm	1.95	13 μm	3.5 μm	3.2

The possible achievable resolution is certainly crucial to reveal the nucleation and growth phenomena at small scales, as the small voids in the void columns are seen here to have sizes around 1 μm. That makes SRCT more suitable than lab CT as smaller length scales can be imaged.

Constitutive relationships for modeling purposes should be based on the mechanics of porous media. In particular, volume variation needs to be accounted for. Finite element modeling based on appropriate constitutive models is needed.[25,26] In classical models, the void volume fraction parameter f, is mainly representative of spherical void growth[27] so that void elongation (shape factor) is badly represented. Figure 10(c) shows that if walls are neglected (supposing that they do not play a mayor micromechanistic role) and the void column is considered to be one single void, the void aspect ratio substantially increases (also see Table 1). Additionally, the anisotropic material deformation behavior (e.g., due to fibril extension) may enhance the elongation of voids. However, these considerations depend on the mechanical strength of the walls, which seems to be unknown at present. The shape and distribution of voids would need to be taken into account. Models accounting for anisotropic void shape and coalescence devoted to metallic materials have been suggested by Gologanu et al.[28,29] These models could be adapted to semicrystalline polymers accounting for anisotropic void growth and coalescence in columns. The quantification of the damage parameters from this study may be used as input/validation data for simulations based on such models. Furthermore, to shed light into the micromechanistic behavior of void columns/clusters and separating walls, unit/periodic cell calculations or even numerical modeling of the microstructure may be performed as in Laiarinandrasana et al.[30]

CONCLUSIONS

The as received PA6 material, and all semicrystalline polymers investigated in earlier studies by the authors, exhibited an initial void volume fraction of about 1%. Tensile tests at room temperature were interrupted to produce necked, whitened samples. Examinations of the microstructure and damage in the necking region via SRCT revealed, for the first time, elongated voids. Further analyses led to the identification of unbroken walls separating voids that are aligned in columns. These observations could be confirmed and refined through a cryo-fractography experiment. The statistical image analysis data of damage parameters was given: the amount of void volume fraction increases from ~1–14% in the necking region. In the necking area the mean Feret dimension aspect ratio is 2 for individual voids (with walls) and 3.2 neglecting walls. More SRCT observations of the different stages of damage evolution are needed to be able to understand voiding process and the final fracture.

The authors would like to acknowledge Elodie Boller, at beamline ID19 at ESRF for help with half acquisition scanning. Anne Laurent is acknowledged for help with cryo-fractography and Franck N'Guyen is gratefully thanked for his contribution to image analysis of SRCT data.

REFERENCES AND NOTES

1 Géhant, S.; Schirrer, R. J Polym Sci Part B: Polym Phys 1999, 37, 113–126.

2 Challier, M.; Besson, J.; Laiarinandrasana, L.; Piques, R. Eng Fract Mech 2006, 73, 79–90.

3 Castagnet, S.; Girault, S.; Gacougnolle, J. L.; Dang, P. Polymer 2000, 41, 7523–7530.

4 Kambour, R. P. J Polym Sci: Macromol Rev 1973, 7, 1–154

5 Kausch, H. H.; Heymanns, N., Plummer, C. J. G.; Decroly, P. Matériaux Polymères: Propriétés Mécaniques et Physiques, Traité des Matériaux, 2001, Vol. 14, Edition: Presses Polytechniques et Universitaires Romande, Lausanne (Switzerland).

6 Butler, M. F.; Donald, A. M.; Ryan, A. J. Polymer 1998, 39, 39–52.

7 Pakula, E.; Fischer, E. W. J Polym Sci: Polym Phys 1981, 19, 1705–1726.

8 Toda, A.; Tomita, C.; Hikosaka, M.; Hibino, Y.; Miyaji, H.; Nonomura, C.; Suzuki, T.; Ishihara, H. Polymer 2002, 49, 947–951.

9 Kramer, E. J. J Appl Polym Sci 1970, 14, 2825–2832.

10 Andrianova, G. P.; Kechekyan, A. S.; Kargin, V. A. J Polym Sci: Polym Phys 1971, 9, 1919–1933.

11 Laiarinandrasana, L.; Besson, J.; Lafarge, M.; Hochstetter, G.; Piques, R. Int J Plast 2009, 25, 1301–1324.

12 Boisot, G. Mechanisms and Mechanical Modelling of Deformation, Damage and Fracture of Neat and Rubber-Toughened PolyAmide 11. PhD Thesis (in French), Ecole Nationale Supérieure des Mines de Paris, France, June, 2009.

13 Regrain, C.; Laiarinandrasana, L.; Toillon, S. Eng Fract Mech 2009, 76, 2656–2665.

14 G'sell, C.; Hiver, J. M.; Dahoun, A. Int J Solids Struct 2002, 39, 3857–3872.

15 Maire, E.; Buffière, J. Y.; Salvo, L.; Blandin, J. J.; Ludwig, W.; Letang, J. M. Adv Eng Mater 2001, 3, 539–546.

16 Morgeneyer, T. F.; Besson, J.; Proudhon, H.; Starink, M. J.; Sinclair, I. Acta Mater 2009, 57, 3902–3915.

17 Maire, E.; Bordreuil, C.; Babout, L. J Mech Phys Solids 2005, 53, 2411–2434.

18 Regrain, C.; Laiarinandrasana, L.; Toillon, S.; Saï, K. Int J Plast 2009, 25, 1253–1279.

19 Parrish, M.; Brown, N. Nat Phys Sci 1972, 237, 122–123.

20 Mazurier, A.; Volpato, V.; Macchiarelli, R. Appl Phys A 2006, 83, 229–233

21 Rasband, W. S. Image J, US National Institutes of Health, Bethesda, Maryland, USA. http://rsb.info.nih.gov/ij/, 1997–2009.

22 Buffière, J. Y.; Proudhon, H.; Ferrie, E.; Ludwig, W.; Maire, E.; Cloetens, P. Nucl Instrum Methods Phys Res B: Beam Interact Mater Atoms 2005, 238, 75–82.

23 Feret, L. R. Assoc Int pour l'Essai des Mat 1932, 2D, 428–436.

24 Regrain, C. Experimental and Numerical Study of Creep Behaviour, Damage and Crack Propagation of Polyamid 6. PhD Thesis (in French), Ecole Nationale Supérieure des Mines de Paris, France, December, 2009.

25 Steenbrink, A. C.; Van der Giessen, E.; Wu, P. D. J Mech Phys Solids 1997, 45, 405–437.

26 Besson, J.; Foerch, R. Comput Methods Appl Mech Eng 1997, 142, 165–187.

27 Koplik, J.; Needleman, A. Int J Solids Struct 1988, 8, 835–853.

28 Gologanu, M.; Leblond, J. B.; Devaux, J. J Mech Phys Solids 1993, 41, 1723–1754.

29 Gologanu, M.; Leblond, J. B.; Devaux, J. Int J Solids Struct 2001, 38, 5595–5604.

30 Laiarinandrasana, L.; Jean, A.; Jeulin, D.; Forest, S. Proceedings of 6th European Conference on Constitutive Models for Rubber, Dresden, Germany, September 7–10th, 2009.